Curing Kinetics and Thermal Property Characterization of *o*-CFER/MeTHPA/O-MMT Nanocomposite

Jungang Gao, Min Zhao, Gang Li

College of Chemistry and Environmental Science, Hebei University, Hebei, Baoding 071002. People's Republic of China

Received 8 April 2005; accepted 30 September 2005
DOI 10.1002/app.23670
Published online in Wiley InterScience (www.interscience.wiley.com).

ABSTRACT: The kinetics of the cure reaction for a system of *o*-cresol-formaldehyde epoxy resin (*o*-CFER), 3-methyltetrahydrophthalic anhydride (MeTHPA), *N,N*-dimethylbenzylamine, and organic montmorillonite(O-MMT) were investigated by means of X-ray diffraction (XRD) and differential scanning calorimetry (DSC). The XRD result indicates that an exfoliated nanocomposite was obtained. The analysis of DSC data indicated the behavior was shown in the first stages of the cure for the system, which could be well described by the model proposed by Kamal. In the later stages, the reaction is mainly controlled by diffusion, and diffusion factor, $f(\alpha)$, was introduced into Kamal's equation. In this way, the curing kinetics was predicted well over the entire range of conversion. Molecular mechanism for curing reaction was discussed. The thermal degradation kinetics of the system were investigated by thermogravimetric analysis (TGA), which revealed that with the increase of O-MMT content, TG curves shift to higher temperature. © 2006 Wiley Periodicals, Inc. J Appl Polym Sci 101: 3023–3032, 2006

Key words: *o*-cresol; epoxy resin; 3-methyl tetrahydrophthalic anhydride; montmorillonite; reaction kinetics; thermal degradation

INTRODUCTION

Composite materials in which inorganic filler is dispersed within the polymer matrix on a nanometer scale are called nanocomposites. These epoxy resin nacomposites have recently been widely studied, principally because of the far-ranging application potential of epoxy resin in many fields.

The nature and mechanism of the exfoliation process of the surface-modified layered-silicate nanoparticles in the crosslinking epoxy network have been of recent interest. Lan[1] demonstrated that the exfoliation of the clay is dependent not only on the reactivity of the epoxy system but also on the rate of intercalation of epoxy and curing agent. Kornmann[2] had compared the effect of aliphatic diamine and cycloaliphatic diamines on the structure of a nanocomposite, and found that the former gave the slowest cure rate, but it allowed more curing agent to penetrate the epoxy swollen galleries and initiate intragallery polymerization, leading to better exfoliation, which may be attributed to its characteristic of a more highly flexible backbone than the cycloaliphatic ones. Monolithic epoxy exfoliated-clay nanocomposites have been prepared from the reaction of alkylammonium-exchanged smectite clays with the diglycidyl ether of bisphenol-A and *m*-phenylenediamine (MPDA) as the curing agent by Pinnavaia and his coworkers.[3] They found that the monolithic exfoliated clay nanocomposite could be formed by preswelling alkylammonium ion exchanged forms of the clays with epoxy resin prior to curing; a tremendous improvement in tensile strength and modulus was realized, particularly when the resin matrix exhibited a subambient glass transition temperature. But the descriptions of synthesis, cure kinetics, and degradation kinetics of *o*-cresol-formaldehyde epoxy resin (*o*-CFER), 3-methyltetrahydrophthalic anhydride (MeTHPA), and organic montmorillonite (O-MMT) nanocomposite system have been lacking until now.

In general, kinetic expressions include two kinds of models: phenomenological and mechanistic. The kinetics of *o*-CFER/MeTHPA/O-MMT system were used to be studied through phenomenological models: the *n*th-order reaction[4] and autocatalytic model.[5] In this article, Kamal's model,[6] arising from an autocatalytic reaction mechanism, was applied to isothermal DSC data.[7–10] In general, a good fit of experimental data was obtained in the early stages of the cure, but deviations were observed in the later stages, particularly near vitrification when the reaction was primarily diffusion controlled. To take into account the diffusion effect, Kamal's model was extended by the introduction of a diffusion factor, $f(\alpha)$. The structure changes during the curing process were investigated by Fourier transform infrared analysis (FTIR) and X-ray diffraction (XRD).[11] Molecular mechanism for curing reaction was discussed. The mechanism of thermal

Correspondence to: J. Gao (gaojg@mail.hbu.edu.cn).

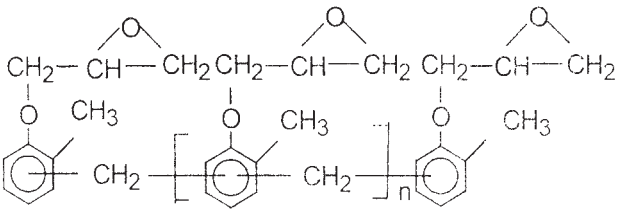

Scheme 1

degradation was studied by means of thermogravimetric analysis (TGA).[12,13]

EXPERIMENTAL

Materials

Epichlorohydrin, *o*-cresol, formaldehyde, NaOH, KOH, acetone, ethyl alcohol, hydrochloric acid, 3-methyltetrahydropathalic anhydride (MeTHPA), *N*,*N*-dimethylbenzylamine were all analytically of pure grade and were supplied by Beijing Chemical Reagent Co. (Beijing, China) Na^+-montmorillonite with the cation exchange capacity (CEC) value of about 100 mmol/100 g was purchased from Qingshan Chemistry Agent Factory (Lin'an, China). $CH_3(CH_2)_{15}(CH_3)_3NBr$, the surfactant of clay, was purchased from the Research Institute of Xinhua Active Material (Changzhou, China).

Preparation of organically modified montmorillonite

Twenty grams of Na^--montmorillonite was dispersed into 500 mL of distilled water at 353 K. Nine grams of $CH_3(CH_2)_{15}(CH_3)_3NBr$ was dispersed in 100 mL distilled water, poured in the hot MMT/water solution, and stirred vigorously for 1 h at 353 K. A white precipitation was formed, and separated by centrifugation, then washed several times with distilled water until no bromide was detected in the filtrate by one drop of 0.1*N* $AgNO_3$ solution. The resulting O-MMT was dried in a convection oven at 353 K. The dried O-MMT was ground with a freezer/mill. The sieved O-MMT powder less than 36 μm was applied for characterization.

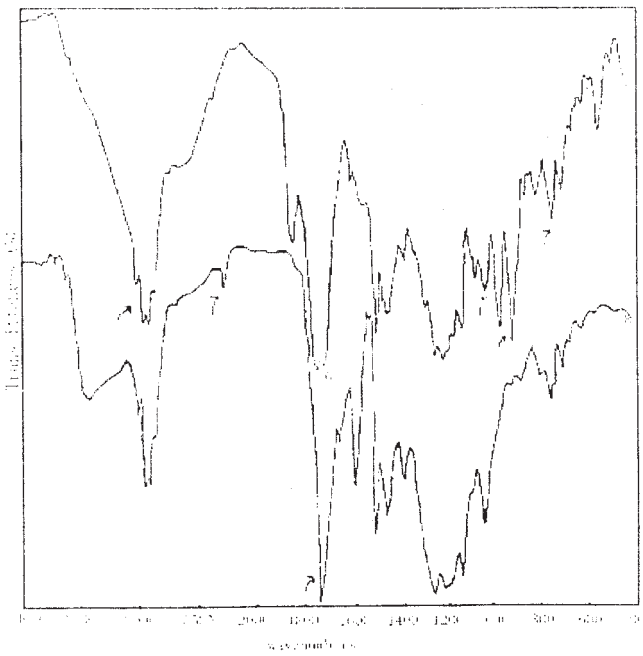

Figure 2 FTIR spectra of nanocomposites after curing at 433 K for (a) noncured *o*-CFER and (b) *o*-CFER cured for 600 min.

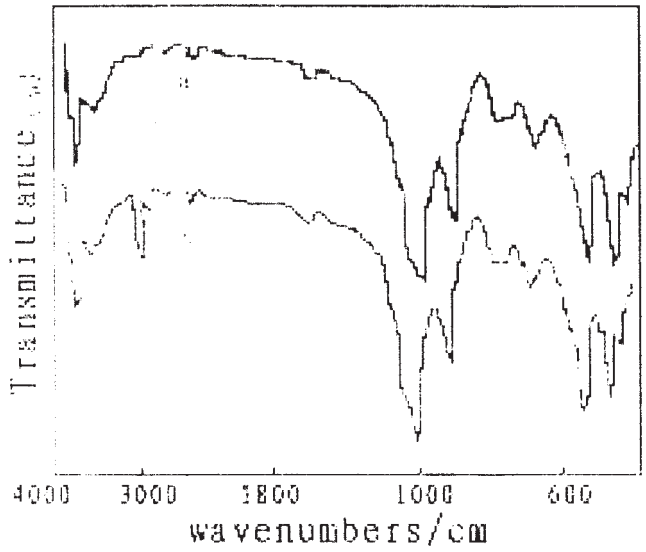

Figure 1 FTIR spectrum of original MMT (a) and organic MMT (b).

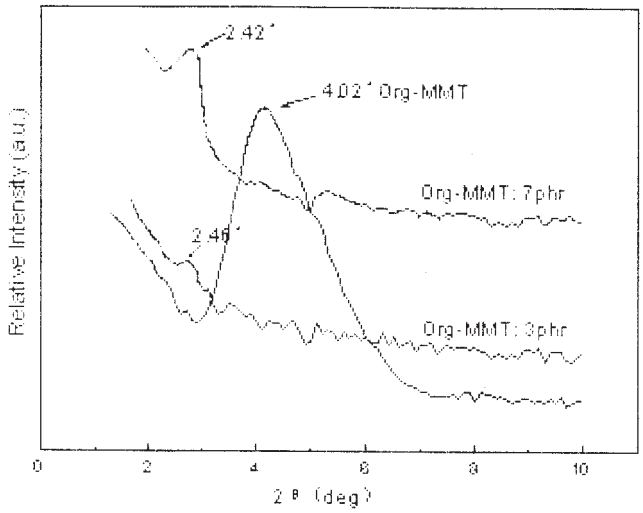

Figure 3 XRD patterns of *o*-CFER/MeTHPA/O-MMT nanocomposites.

TABLE I
Experimentation Data of Cure Reaction

Sample	Temperature of peak (K)			Enthalpy	Curing time
	T_i	T_p	T_f	ΔH (J/g)	(t/min)
o-CFER/MeTHPA	353	406	455	175.3	10
o-CFER/MeTHPA/O-MMT	353	407	456	174.5	10

Synthesis of *o*-CFER

Epoxy resin based on *o*-cresol-formaldehyde epoxy resin (*o*-CFER) was synthesized according to refs. 14 and 15 The line *o*-cresol-formaldehyde resin synthesized in the first step was reacted with epichlorohydrin in the second step. The molecular structure of this epoxy resin has the approximate form of Scheme 1.

Where n = 1–3. The epoxy value was determined according to Jay [16] to be 0.357 mol/100 g.

Synthesis of *o*-CFER/MeTHPA/O-MMT nanocomposites

The *o*-CFER was mixed with the desired amount of O-MMT. The O-MMT was dispersed uniformly in *o*-CFER at 353 K for 2 h. Then, curing agent was added into the hybrid and mixed thoroughly by stirring. The mixtures were freed of bubbles by vacuum after they were cast into a mold. The ratio of *o*-CFER and MeTHPA is 1 : 1*M* ratio of carboxyl group to epoxy group, and the *N*,*N*-dimethyl-benzylamine was used as curing accelerant. The loadings of filled O-MMT were 0, 3, and 7 phr (per 100 phr resins mixtures), respectively. The samples were cured for 2 h at 403 K and for 4 h at 433 K.

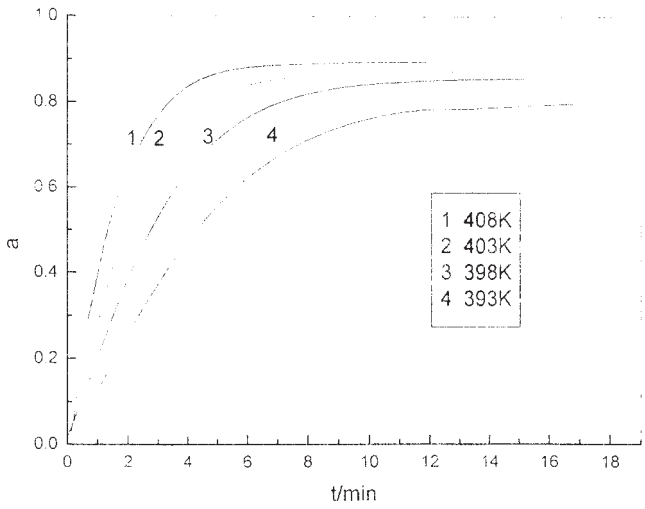

Figure 4 Conversion α versus time plots at different curing temperatures.

Ir measurements

The *o*-CFER/MeTHPA/O-MMT samples were prepared with a stoichiometric ratio of one epoxy group to one carboxyl group. An FTS-40 IR spectrophotometer (FTIR, BIO-RAD Co.) was used for the investigation of the structural changes of the curing system.[17] The sample was dissolved in acetone, and then coated as a thin film on a potassium bromide plate. Acetone was completely evaporated in vacuum. The sample was cured in a heated oven with a fixed temperature of 433 K. The noncured sample, cured sample, the pristine montmorillonite, and organic montmorillonite were analyzed by FTS-40 IR spectrophotometer, respectively.

X-ray diffraction (XRD)

X-ray diffraction patterns were recorded by monitoring the diffraction angle 2θ from 1.5° to 10° on a RigakuD-max-γA-ray diffractometer. The diffractometer was equipped with a Cu Kα (λ = 0.1542 nm) radiation source operated at 40 kV and 100 mA. The scanning speed and the step size used were 2°/min and 0.02°, respectively.

DSC measurements

DSC analysis was carried out on a DT-41 differential scanning calorimeter (DSC) (Shimadzu Co. Ltd., Japan). The DSC instrument was calibrated with high-purity indium. α-Al_2O_3 was used as the reference material. Isothermal and dynamic heating experiments were carried out according to Opalicki et al.,[7] under a nitrogen flow of 40 mL min^{-1}.

About 10 mg of samples weighed accurately was placed into an aluminum DSC sample pan and sealed with an aluminum lid. The entire operation was carried out in a dry chamber. Isothermal DSC was performed at a series of curing temperatures T_c, 393, 398, 403, and 408 K, respectively. The reaction was considered complete when the rate curve leveled off to the baseline. The total area under the exothermal curve, based on the extrapolated baseline at the end of the reaction, was used to calculate the isothermal heat of cure, ΔH_i, at a given temperature. After each isothermal run, the sample was quenched rapidly to 283 K

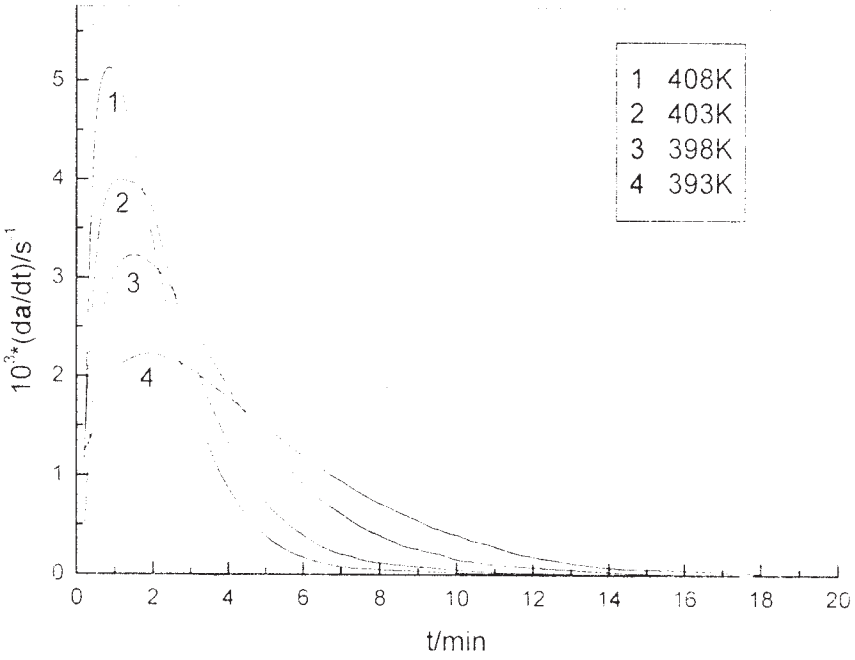

Figure 5 Reaction rate $d\alpha/dt$ versus time plots at different temperatures.

and then reheated at 10 K min^{-1} to 573 K to determine the residual heat of reaction, ΔH_r. The total heat evolved during the curing reaction is $\Delta H_0 = \Delta H_i + \Delta H_r$.

Thermogravimetric analysis measurement (TGA)

The sample was cured at 433 K for 4 h and the thermal analysis was carried out on a Shimadzu DT-40 thermogravimetric analyzer under a static air atmosphere. About 3 mg of the sample, which had been completely cured, was put into a platinum cell and placed on the detector plates, and then the furnace was heated to 923 K at a heating rate of 10 K min^{-1}.

RESULTS AND DISCUSSION

FTIR analysis

Figure 1 shows the infrared spectra of the pristine montmorillonite and organ montmorillonite. FTIR spectra of the *o*-CFER/MeTHPA/O-MMT system are shown in Figure 2. The IR spectra of nanocomposites reveal the presence of characteristic absorptions of both inorganic and organic components. The absorption peaks at 1039 and 796 cm^{-1} of MMT can be associated with Si—O—Si stretching vibrations. Absorption bands, on the other hand, at 3000–2800 cm^{-1} (CH_2 stretching), 1750 cm^{-1} (carbonyl group vibration), 1620–1436 cm^{-1} (aromatic C═C stretching), and 950–750 cm^{-1} (epoxide ring vibration) are consequences of the epoxy polymer. Especially, a new peak at 3000–2900 cm^{-1} appeared because of the CH_2 mode in the O-MMT. It is indicated that the MMT interlayer has been organically modified by $CH_3(CH_2)_{15}(CH_3)_3NBr$.[18–20] The most significant feature is the epoxide group absorption at 914 cm^{-1} (marked by an arrow). This absorption peak of *o*-CFER/MeTHPA/O-MMT cured for 600 min at 433 K becomes much lower than that of the noncured *o*-CFER. In addition, the IR absorption in the carbonyl group of MeTHPA is a bipeak at about 1750 cm^{-1} before curing, but it became a single peak after curing. It is shown that this reaction can be completed at 433 K for over 600 min.

TABLE II
Kinetic Parameters for Isothermal Curing Reaction of *o*-CFER/MeTHPA/O-MMT

T (K)	k_1 (10^{-4} S^{-1})	k_2 (10^{-3} S^{-1})	m	n
393	2.03	6.02	11.73	20.94
398	4.68	7.21	12.02	18.83
403	0.38	0.45	0.47	0.76
408	1.17	1.26	1.44	1.89

X-ray diffraction analysis

The X-ray diffraction patterns for *o*-CFER/MeTHPA/O-MMT composites containing different content of O-MMT cured under the temperature of 433 K are shown in Figure 3. As reported,[21] when polymer chains are inserted into the galleries of montmorillonite, the lattice spacing is enlarged. These XRD patterns reveal the change in O-MMT basal spacing that occurs in the epoxy curing process. For the *o*-CFER/

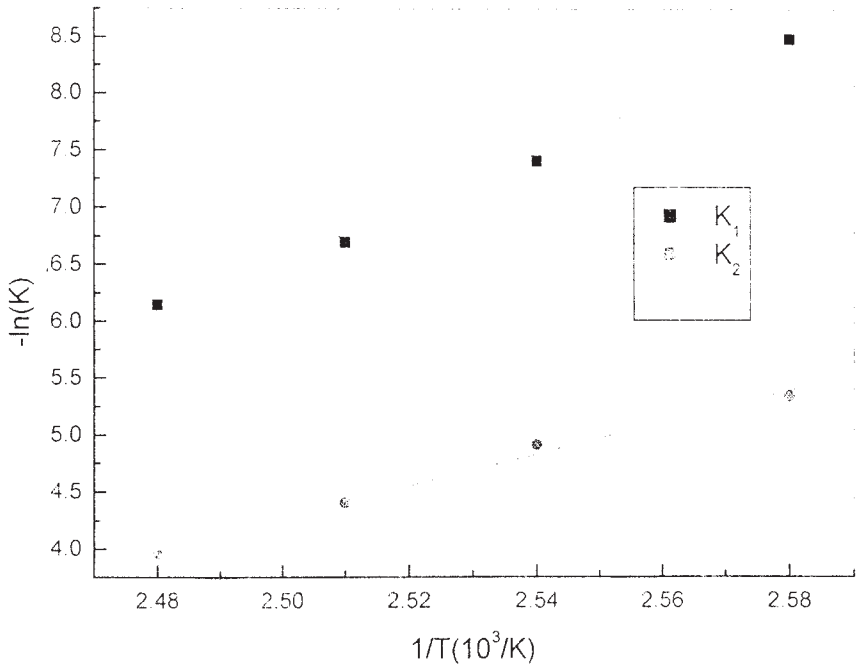

Figure 6 Rate constants of curing reaction, k_1 and k_2, versus temperature.

MeTHPA/O-MMT system, it is noteworthy that the (001) diffraction peak, corresponding to the basal spacing of montmorillonite d_{001}, shifted to a lower angle comparable to that of O-MMT, and the peak intensity increased with increased loading of O-MMT. The X-ray diffraction peak occurs at $2\theta = 4.02°$ for O-MMT, and for the *o*-CFER/MeTHPA/O-MMT composite the peak of diffraction appeared at $2\theta = 2.42°$ –2.46°. Obviously, the intercalated nanocomposite with the lattice spacing of 3.59–3.65 nm (according to $2d \sin \theta = n\lambda$) was obtained. As Pinnavaia pointed out, the lattice spacing of the intercalated nanocomposite increases, but Bragg diffractions still exist in the diffractogram, which shifted to lower angle. If the lattice spacing continues to increase, exfoliated nanocomposite is formed, leading to the disappearance of Bragg diffraction.

The heat (δh) of cure reaction of nanocomposites

The DSC experiment was carried out by dynamic method, mensurating the heat of different O-MMT content according to the literature.[22] It was found that the addition of O-MMT had little effect on the reaction. Table I lists the heat parameters. It is indicated that the curing temperature region, enthalpy, and curing time are all the same for *o*-CFER/MeTHPA and *o*-CFER/METHPA/O-MMT, obviously, and addition of O-MMT has no effect on the curing reaction of O-CFER/MeTHPA. However, because of the addition of O-MMT, the thermal stability, flame retardancy, and mechanic properties were increased.

Isothermal curing DSC

The mechanisms of the curing reaction of thermosetting resins have two general kinetic models: *n*th-order kinetics and autocatalytic kinetics [12]. The reaction rate of *n*th-order kinetics can be expressed as

$$\frac{d\alpha}{dt} = K(T)(1 - \alpha)^n \tag{1}$$

The reaction rate of autocatalytic kinetics can be defined as

$$\frac{d\alpha}{dt} = k'\alpha^m(1 - \alpha)^n \tag{2}$$

where α is the extent of reaction given by $\alpha = \Delta H_t / \Delta H_0$, where ΔH_t is the partial area under a DSC trace up to time t; m and n are the reaction orders; and k' is the kinetic rate constant.

To take into account the autocatalytic reaction, where the initial reaction rate of the autocatalytic reaction is not zero, Kamal [6] proposed the following generalized expression.

$$\frac{d\alpha}{dt} = (k_1 + k_2\alpha^m)(1 - \alpha)^n \tag{3}$$

where k_1 and k_2 are the specific rate constants, which are functions of the temperature. According to the *n*th-order kinetic model, the maximum reaction rate will be observed at $t = 0$, and according to the auto-

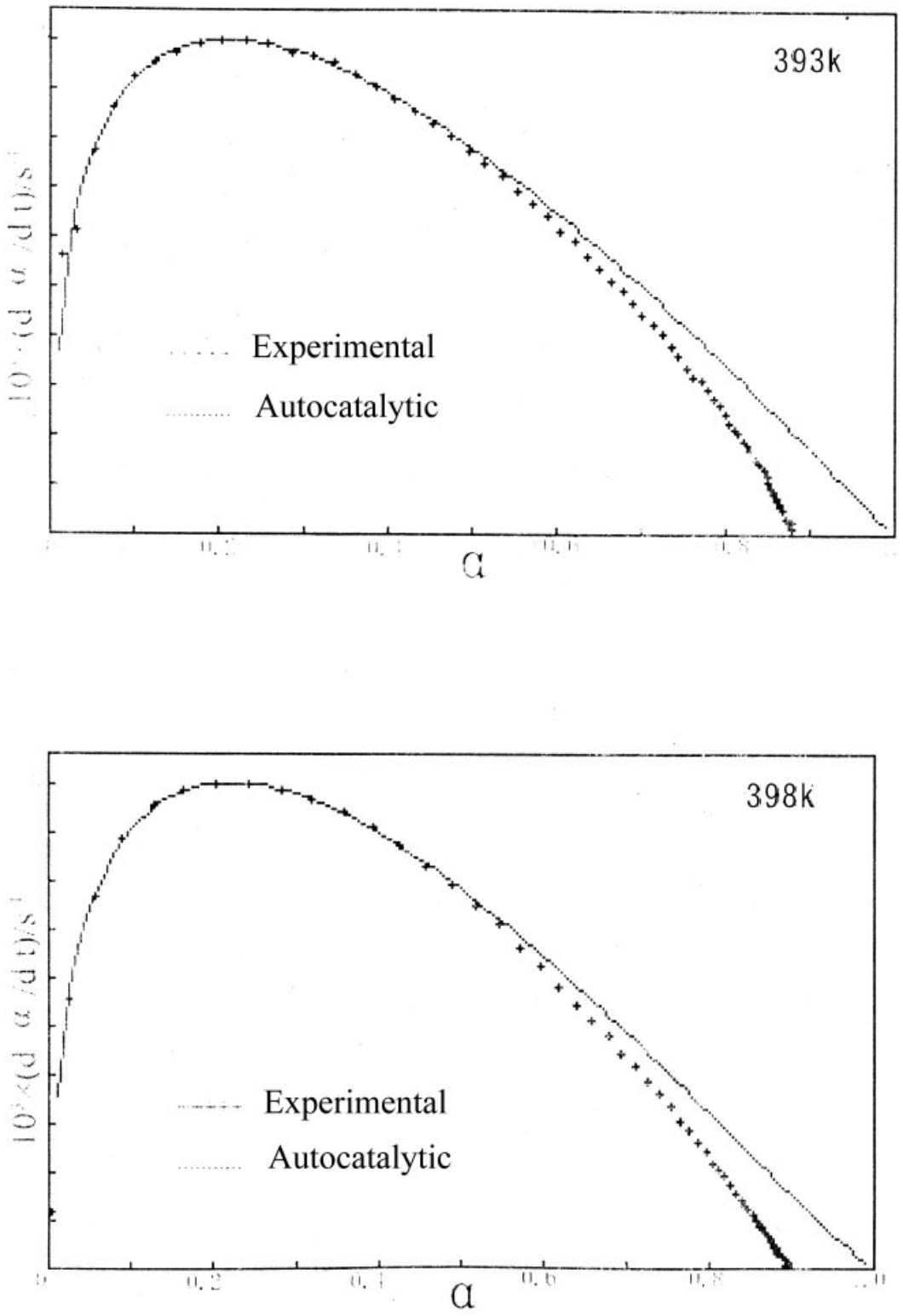

Figure 7 Comparison of experimental data with theoretical values: plots of reaction rate $d\alpha/dt$ versus conversion α at 393 and 398 K

catalytic model, the reaction rate is zero initially and attains the maximum value at some intermediate conversion.

During the curing reaction of thermosetting resins, the heat evolution recorded by DSC is proportional to the extent of consumption of the epoxide groups in the epoxy resins, or the reactive groups in the curing agent,[23,24] that is, the released heat is proportional to the extent of the reaction. Following this assumption, the curing kinetics was studied, and the kinetics data

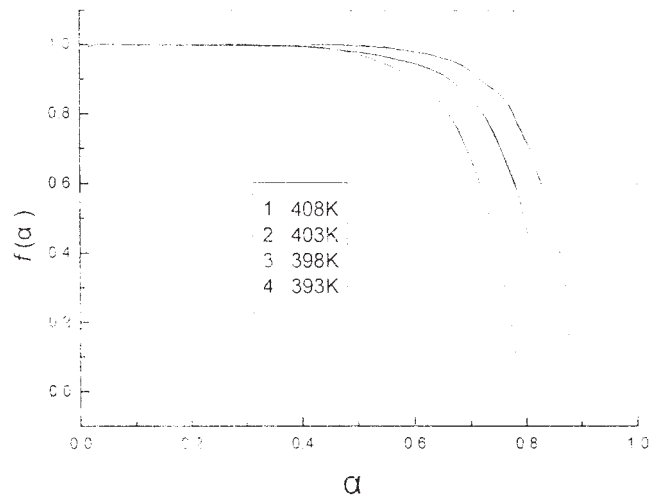

Figure 8 Plots of diffusion factor $f(\alpha)$versus conversion α at different curing temperature.

was determined. If the cure reaction is the only thermal event, then the reaction rate $d\alpha/dt$ is proportional to the heat flow,[12] dH/dt, that is,

$$\frac{d\alpha}{dt} = \frac{dH/dt}{\Delta H_0} \tag{4}$$

The rate of cure can be determined by the curing exotherm, Figure 4 shows the plots of curing reaction conversion α versus time t at different isothermal temperatures, and the plots of $d\alpha/dt$ versus time t are shown in Figure 5. As seen from Figure 4 and 5, the reaction rate at any temperature increases with time at the initial stage of cure and passes through a maximum. The peak of reaction rate becomes higher and shifts to shorter time with an increase in curing tem-

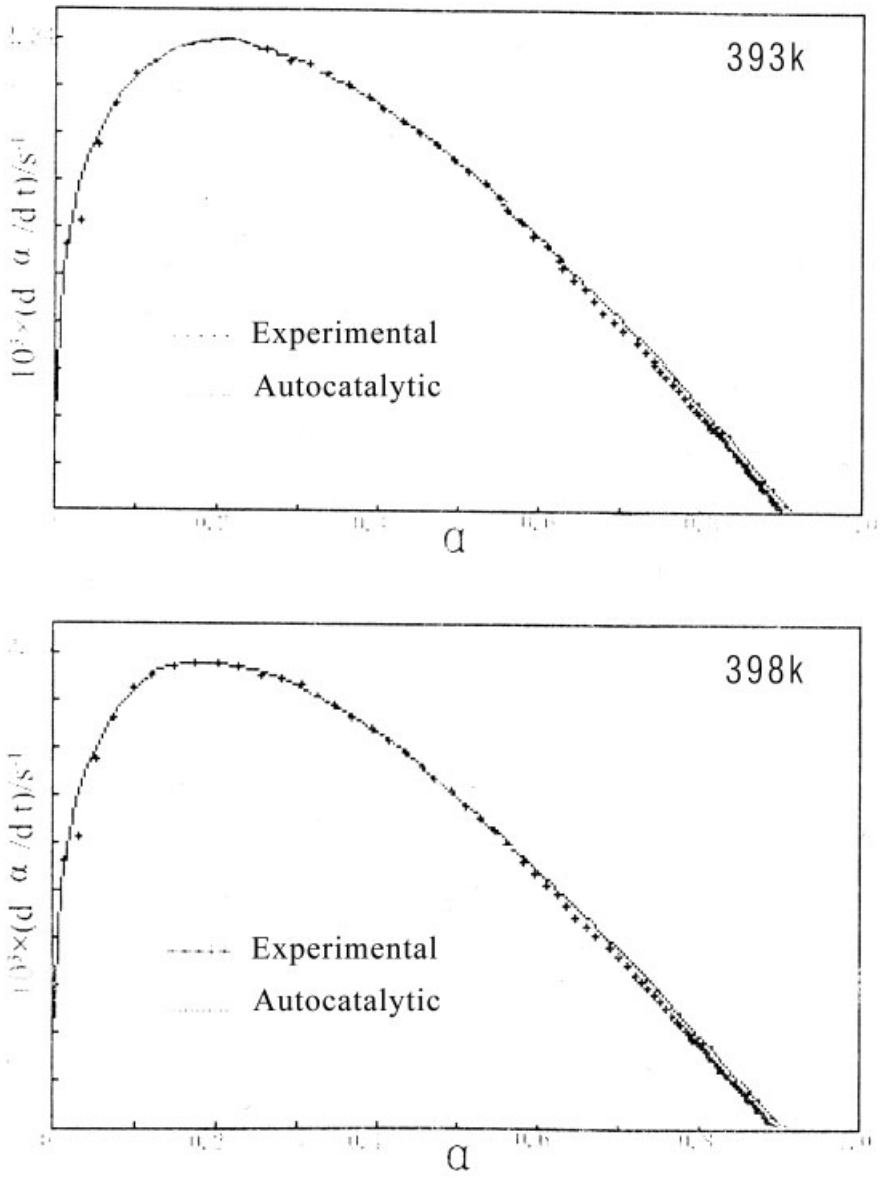

Figure 9 Comparison of experimental data with theoretical values calculated from eq. (7): reaction rate $d\alpha/dt$ versus conversion α at 393 and 398 K.

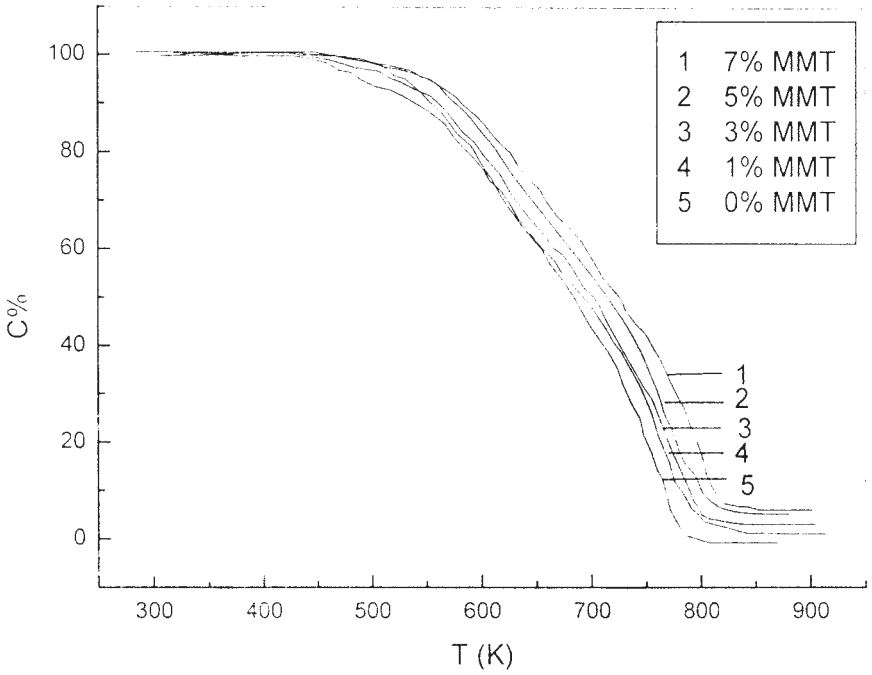

Figure 10 The thermal degradation curves of nanocomposites with different O-MMT content.

perature, but the conversion α reaches only about 80–90% in the experiment time. The plots show a maximum reaction rate at time $t > 0$, thereby negating simple nth-order kinetics. To compute kinetic parameters in eq. (3), several methods have been proposed.[25–27] In this study, k_1 was graphically calculated as the initial reaction rate at time $t = 0$, given by the intercept of Figure 5. Then, k_2, m and n were calculated through nonlinear regression, according to eq. (3). The resulting data are shown in Table II.

It can be seen from Table II that k_1 values are small compared with the k_2 values, which affects the reaction more. Furthermore, k_1 and k_2 values increase with the increase in curing temperature. The reaction rate constants k_1 and k_2 depend on the temperature and follow the Arrhenius relationship

$$k_i = A_1 \exp(-E_1/RT)\ i = 1.2 \qquad (5)$$

where A_i is the pre-exponential constant, E_i is the activation energy, R is the gas constant, and T is the absolute temperature. Rate constants k_1 and k_2 are shown as Arrhenius plot in Figure 6; the values of associated activation energies E_1 and E_2 are 188.94 and 114.93 kJ/mol, respectively. The linear correlation coefficient is 0.9973 for k_1 values and 0.9958 for k_2.

Typical comparisons between the experimental DSC data for two different temperatures 393 and 398 K, and the autocatalytic model with eq. (3) determined parameters are shown in Figure 7. The kinetics behavior described by the kinetic model coincides with the experimental data in the early stage. As the reaction progresses, a deviation appears due to the onset of gelation and vitrification in which the mobility of reactive groups is hindered, and the rate of conversion is controlled by diffusion rather than by kinetic factors.[28] Differences between model predictions and experimental data were observed. This can be interpreted in terms of free volume considerations.[29] The free volume of materials decreases with temperature, and then the rate of diffusion of reactive groups is reduced, leading to decrease in reaction rate.

To consider the diffusion effect more precisely, a semiempirical relationship, based on free volume considerations, was proposed by Chern and Poehlein.[29] In this relationship, a diffusion factor, $f(\alpha)$, is defined with two empirical parameters as follows:

$$f(\alpha) = \frac{1}{1 + \exp[C(\alpha - \alpha_c)]} \qquad (6)$$

where C is the diffusion coefficient and α_c is the critical conversion depending on the curing temperatures. The plots of $f(\alpha)$ versus conversion α at different curing temperatures are shown in Figure 8. For $\alpha << \alpha_c$, $f(\alpha)$ approximately equals unity and the effect of diffusion is negligible, so that the reaction is kinetically controlled. As α approaches α_c, f(α) begins to decrease, reaching a value of 0.5 at $\alpha = \alpha_c$. Beyond that point, it continues to decrease and approaches zero, which means that the reaction becomes very slow and effectively stops.

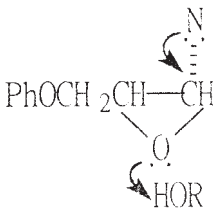

Scheme 2

Considering the diffusion effect, the kinetics equation of cure can be expressed in the following form to account for the effects of diffusion.

$$\frac{d\alpha}{dt} = (k_1 + k_2\alpha^m)(1 - \alpha)^n \cdot \frac{1}{1 + \exp[C(\alpha - \alpha_c)]} \quad (7)$$

Figure 9 shows the comparison between experimental values and those obtained from eq. (7). The calculated values agree very well with experimental data under higher temperature.[30] Therefore, we employ the proposed generalized kinetic model to predict and describe the advance of this epoxy resin systems as a function of the curing temperature.

Thermal degradation

The process of weight loss is shown in Figure 10. It can be seen that with the increase of O-MMT content, TG curves shift to higher temperatures, and the corresponding temperatures T_{max} at the maximal degradation velocity increased, too. When the content of O-MMT is 7%, the T_{max} are 33.6 K higher than that of pure *o*-CFER/MeTHPA system. The thermal stability of composites improved, attributing to the fact that the layers of O-MMT suppressed the emanation of the small molecule effectively when degradation reaction originated, resulting in the decrease of degradation velocity of the composites. In addition, the stronger interaction between *o*-CFER and O-MMT confined the activity of the macromolecule chains, and thus improved the heat resistance of the composites.

Molecular mechanism for curing reaction

It is known that the addition of hydroxyl containing compounds (water, alcohols, phenols et al.) considerably promotes the interaction of epoxy compounds with anhydrides, amines, and other nucleophilic attack. The reaction proceeds through a trimolecular transition state, initially suggested by Smith [31] for the reaction of epoxy compounds with amines (Scheme 2).

As reported,[32] the maximum curing reaction rate was observed at $t = 0$ in the presence of hydroxyl containing solvent and obeyed *n*th order kinetics. This is due to the participation of proton. As to the pure epoxy resin/anhydride system, the curing reaction is given as the following formula in Scheme 3.

Then the oxygen negative ion reacts with epoxy group. Tertiary amine is not reformed in the reaction. Because of the participation of hydroxyl group in the macromolecular chain, the k_1 is not zero and is also not the typical catalysis mechanism. The hydroxyl group come from little unreacted hydroxyl of phenolic and

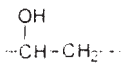

produced by the reaction of epoxy group with hydroxyl of phenolic. It is favorable for the —OH in the epoxy resin molecular chain to become proton donor and participate in the reaction with the increasing curing temperature. The reaction mechanism ought to become trimolecular mechanism with the participation of the proton. This is the reason that the m + n values increase with the temperature.

CONCLUSIONS

The XRD indicates that the epoxy resin molecules have been inserted into the galleries of montmorillon-

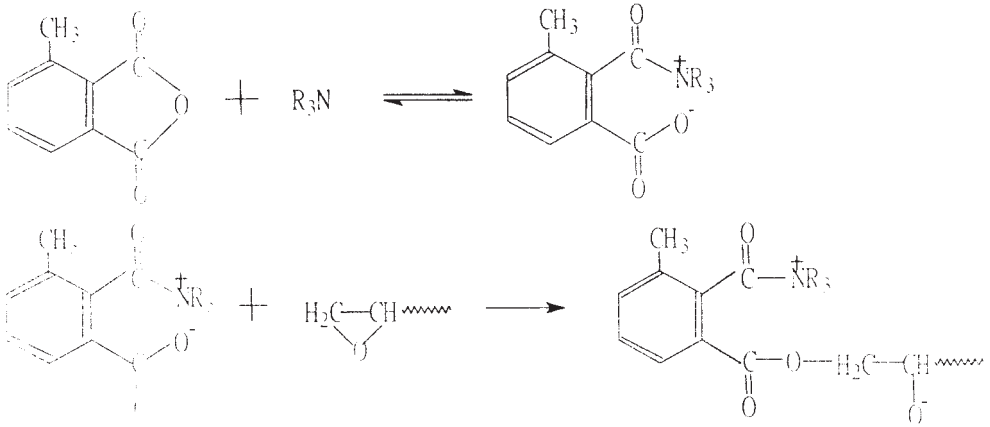

Scheme 3

ite and an exfoliated nanocomposite was obtained. The O-MMT has not changed the reaction mechanism of *o*-CFER/MeTHPA. The cure reaction of *o*-CFER/MeTHPA/O-MMT system shows an autocatalytic kinetic behavior in the kinetically controlled stage and can be well-described with the model proposed by Kamal. The curing reaction at the later stage was practically diffusion-controlled. To consider the diffusion effect more precisely, diffusion factor $f(\alpha)$ was introduced into Kamal's equation to make it possible to describe and predict the cure reaction of this epoxy resin. The theoretical values agree very well with the experimental data. With the increase of O-MMT content, TG curves shift to higher temperature, and the corresponding temperatures at the initial degradation and at the maximal degradation velocity increased.

References

1. Lan, T.; Kaviratna, P. D.; Pinnavaia, T. J. Chem Mater 1995, 7, 2144.
2. Kornmann, X.; Lindberg, H.; Berglund, L. A. Polymer 2001, 42, 4493.
3. Lan, T.; Kaviratna, P. D.; Pinnavais, T. J. Proc ACS Div Polym Mater Sci Eng 1994, 71, 528.
4. Deng, B. L.; Hu, Y. S.; Chen, L. W.; Chiu, W. Y.; Wu, T. R. J Appl Polym Sci 1999, 74, 229.
5. Lam, P. W. K.; Plaumann, H. P.; Tran, T. J Appl Polym Sci 1990, 41, 3043.
6. Kamal, M. R. Polym Eng Sci 1974, 14, 23.
7. Opaticki, M.; Kenny, J. M.; Nicolars, L. J Appl Polym Sci 1996, 61, 1025.
8. Khanna, U.; Chanda, M. J Appl Polym Sci 1993, 49, 319.
9. Duswalt, A. A. Thermochim Acta 1974, 8, 57.
10. Wang, M. W.; Lee, C. T.; Lin, M. S. Polym Int 1997, 44, 503.
11. Stevens, G. C. J Appl Polym Sci 1981, 26, 4279.
12. Liu, Z. Introduction of Thermal Analysis. Chem Industry Publishing Co: Beijing, 1991; p 100.
13. Madhusudanan, P. M.; Krishnan, K.; Ninan, K. N. Thermochim Acta 1986, 97, 189.
14. Ren, L. B. Thermosetting resin 1998, 13, 17.
15. Wang, C. S.; Liao, Z. K. Polym Bull 1991, 25, 559.
16. Jay, R. R. Anal Chem 1964, 36, 665.
17. Hong, S. G.; Wu, C. S. J Therm Anal Cal 2000, 59, 711.
18. Lan, T.; Kaviratna, P. D.; Pinnavaia, T. J. J Phys Chem Solids 1996, 57, 1005.
19. LeBaron P. C.; Wang, Z.; Pinnavaia, T. J. Appl Clay Sci 1999, 15, 11.
20. Lan, T.; Pinnavaia, T. J. Chem Mater 1996, 8, 1584.
21. Kornmann, X.; Lindberg, H.; Berglund, L. A. Polymer 2001, 42, 1303.
22. Yang, X. W.; Yin, J.; Li, F. Y.; Journal of Tianjin Urban Construction Institute 1994, 4, 30.
23. Woo, E. M.; Seferis, J. C. J Appl Polym Sci 1990, 40, 1237.
24. Ghaemy, M.; Riahy, M. H. Eur Polym Mater 1996, 32, 1207.
25. Ryan, M. E.; Dutta, A. Polymer 1979, 20, 203.
26. Moroni, A.; Mijiovic, J.; Pearce, F. M.; Foun, C. C. J Appl Polym Sci 1986, 32, 3761.
27. Kenny, J. M. J Appl Polym Sci 1994, 51, 761.
28. Cole, K. C.; Hechler, J. J.; Noel, D. Macromolecules 1991, 24, 3098.
29. Chem, C. S.; Poehlein, G. W. Polym Eng Sci 1987, 27, 782.
30. Gao, J. G.; Li, Y. F. Polym Int 2000, 49, 1590.
31. Smith, I. T. Polymer 1961, 2, 95.
32. Liu, T. D.; Wang, Q. C.; Xu, X. P. Thermosetting resin 1989, 2, 38.